IEEE Access
Multidisciplinary | Rapid Review | Open Access Journal

Received April 6, 2018, accepted May 11, 2018, date of publication May 18, 2018, date of current version June 20, 2018.

Digital Object Identifier 10.1109/ACCESS.2018.2838446

Determination of Core Losses in Open-Core Power Voltage Transformers

IGOR ŽIGER[1], (Member, IEEE), BOJAN TRKULJA[2], AND ŽELJKO ŠTIH[2], (Member, IEEE)
[1]Končar–Instrument Transformers. Inc., 10090 Zagreb, Croatia
[2]Faculty of Electrical Engineering and Computing, University of Zagreb, 10000 Zagreb, Croatia

Corresponding author: Igor Žiger (igor.ziger@koncar-mjt.hr)

ABSTRACT Power voltage transformers (PVTs) are becoming increasingly present in different substation solutions on a world scale. Such units that are based on the open-core concept introduce several advantages in terms of transformer performance and reliability. This paper provides context for distinct open-core losses, expanding in detail on a measurement-based method for determining both total and specific losses in the open core. The approach is demonstrated on several core model configurations with varying parameters. Apart from loss measurement, the presented core configurations were used to determine and verify the distribution and magnitude of all flux density vector components. The proposed approach is validated by various accompanying measurements but also through comparison with loss measurements performed on several PVT units intended for commercial application.

INDEX TERMS Finite elements method, instrument transformers, loss measurement, open-core concept, magnetic flux density, magnetic field measurement, power voltage transformers, transformer cores.

I. INTRODUCTION AND MOTIVATION

Power Voltage Transformers (PVTs), also known as Station Service Voltage Transformers or Auxiliary Service Voltage Transformers, are an expanding product niche, both for auxiliary power and rural electrification applications [1], [2].

PVTs are primarily instrument transformers by design philosophy and technology of production, meaning they are currently defined by standards applicable to instrument transformers [3]. These standards typically specify 55 °C temperature rise class.

Contrary to their instrument transformer counterparts, accompanying losses generated in PVTs are not insignificant, meaning that both loss determination techniques and methods for their reduction become increasingly important.

Using the open-core concept as a foundation for PVT design results in a number of advantages in terms of service performance and transformer reliability. These advantages entail a ferroresonance-immune design, inherent internal fault safety, inrush current elimination and a robust insulation system, highly insusceptible to overvoltages of various character and origin [4], [5]. The design outline and main components of open core units are disclosed in detail in [4] and [5].

On the other hand, the specialties of open core concept with respect to transformer losses are not widely known. In this paper, the focus is placed on determination of the losses in the open core itself, as it is the most significant challenge.

The primary goal is to present a novel, measurement-based methodology for evaluation of open core losses. The method is based on core loss measurements, conducted in a testing circuit developed specifically for that purpose, which are then post-processed with Finite Element Analysis (FEA) software.

The method is validated through flux density distribution measurements, performed on several core models which were assembled in different configurations with varying parameters. Finally, the method is corroborated by measurements on several PVT units intended for commercial application, which confirms its adequacy as a valid, useful and minimally time-consuming approach intended for application at the industry level.

II. PROBLEM DEFINITION

A typical example of the open-core geometry, along with its main identifying parameters can be seen in Fig. 1(a). Apart from those parameters, the two main variables that define the open core are the utilization factor K_U and the form factor K_F. Utilization factor K_U is defined by equation (1), and represents the ratio between the net cross-sectional area S_{Fe} and the gross area of the core circle with a diameter of $\emptyset_{limb}$.

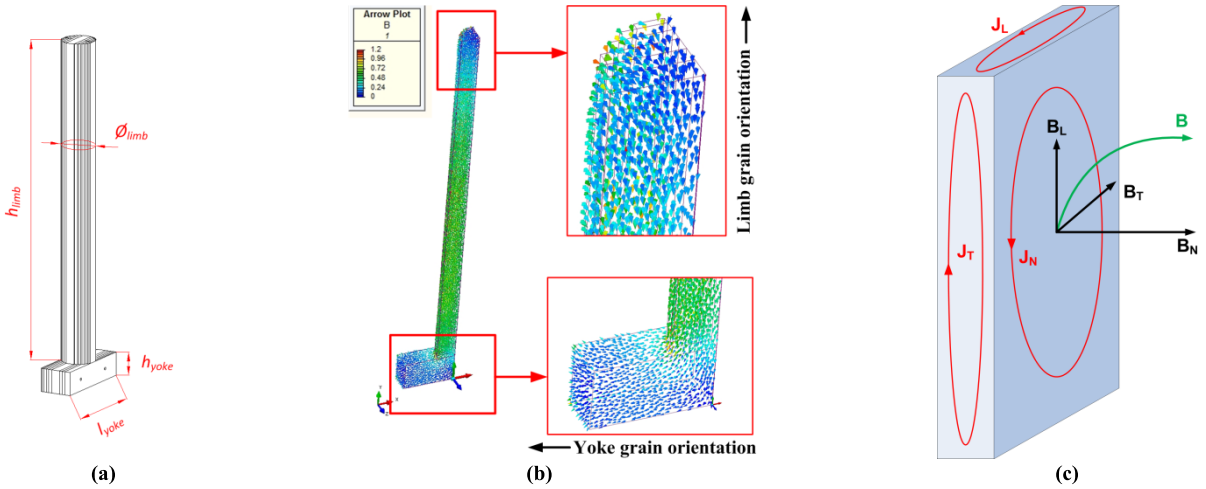

FIGURE 1. (a) Open core geometry with identifying parameters (b) Typical flux density distribution in the open core (c) Simplified representation of flux density vector components and corresponding eddy currents that appear in a single lamination.

Form factor K_F is defined as the ratio of the mean flux path length l_{Fe}, and the core limb diameter $\emptyset_{limb}$, as shown in equation (2). Mean flux path length l_{Fe} is defined in equation (3).

Typical values of K_U are in the range of 0.5-0.95 and K_F in the range of 5-20, depending on core geometry and specific product requirements. All cores considered in this paper had a stacking factor of 0.9593, according to the information provided by the core manufacturer and were made from the same M140-35S material.

$$K_U = \frac{4 \cdot S_{Fe}}{\emptyset_{limb}^2 \cdot \pi} \tag{1}$$

$$K_F = \frac{l_{Fe}}{\emptyset_{limb}} \tag{2}$$

$$l_{Fe} = h_{limb} + \frac{h_{yoke} + l_{yoke}}{2} \tag{3}$$

Due to a significant field path through the air surrounding the open-core limb, as shown in Fig. 1(b), the magnetizing current is practically independent on the core material, as the portion of the current needed to magnetize the laminated steel material is negligible in comparison to the portion of the current needed to magnetize the air [5].

A typical flux density distribution in the open core, shown on a representative core model with 1/4 symmetry, calculated with anisotropic material properties can be seen in Fig. 1(b).

It can be seen that the flux density vector is oriented in various directions with respect to the core lamination orientation direction, while also containing a significant component which is perpendicular to the lamination itself. These two effects cause additional losses to appear in the open-core. A simplified representation of these effects can be seen in Fig. 1(c). Flux density vector can be divided into three components, B_L, B_N and B_T. B_L is the component parallel to lamination orientation direction, B_N is the normal component, perpendicular to the lamination surface, while B_T is the tangential component.

Flux density vector components cause narrow eddy current loops in the rolling plane, labeled J_L and J_T, respectively. In conventional closed core transformers, these loops are generally predominant [6], [7]. In contrast, with the open core, the predominant eddy current loops J_N are caused by the normal component of the flux density vector (B_N).

The considered range of flux density is a consequence of typical continuous operating conditions of PVTs. Due to the continuous and short-term voltage factors, which can range from 1.1 to 2.2 times the rated voltage, the rated flux density in these units is comparatively lower than in conventional distribution or power transformers [3]. Therefore, the rated peak flux density range of interest is between 0.9 and 1.35 T.

All effects considered in this paper are confined to the rated frequency of 50 Hz.

III. APPROACH

Losses in laminated media have been thoroughly investigated by different researchers over a long period of time for various applications [8]–[15].

As individual laminates are difficult to model using available 3D FEM solvers, there are several different approaches to bypass these obstacles [9], [12]. One approach is to introduce a two-step method, consisting of modeling anisotropic magnetic material parameters to obtain the correct field distribution, and then correcting the resulting eddy current losses by taking into account the local field in the laminates as well as edge effects [8]–[10].

Also, homogenization methods can be used, yielding accurate flux density distributions, and less accurate loss prediction, especially at higher flux density values [13]. Cheng *et al.* [16], [17] are proposing partial homogenization of the laminated media, with the first few laminations modeled individually and the rest of the laminations modeled as bulk material with anisotropic properties.

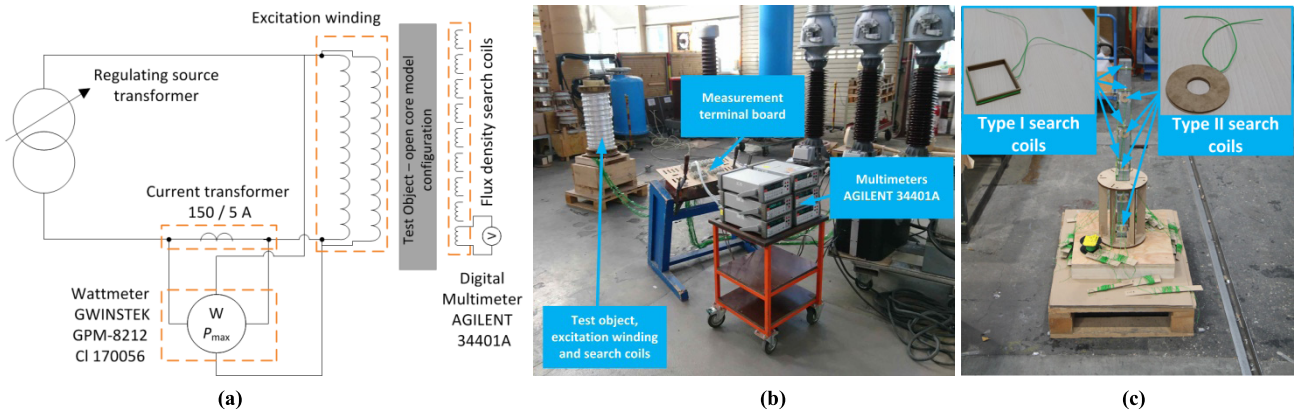

FIGURE 2. (a) Measurement circuit (b) Test setup in the testing laboratory (c) Assembled individual core model equipped with search coils.

On the other hand, commercial FEM solvers, still implement models based on variations of the Steinmetz hysteresis loss model, usually expanded into a three component loss model including hysteresis, eddy current and additional, or excess loss [6]. The interdependence of these phenomena brings the loss separation models in question. However, due to their widespread application and ease of use this approach remains very popular.

In transformer design process, quickly obtainable results based on empirical and semi-empirical approaches are also utilized. In conventional closed core transformers, core losses can be determined using predefined specific loss curves provided by electrical steel manufacturers and correcting those values with an empirically-based building factor, which includes all loss components not included in the nominal loss curve, such as extra losses in joint regions, interlaminar losses, burr, air gaps, local saturation, etc.

Different aspects of the building factor can be calculated beforehand [18], [19].

However, the specific losses of the open core differ with the core geometry and the geometry of the winding magnetizing the core, meaning that the predefined material loss curves are not sufficient. Additionally, intricate eddy current loss calculating techniques discussed in [8]–[15] are often optimized for a certain geometry and not completely applicable to the open core.

Moreover, while these methods may be accurate in determining eddy current losses, other discrete losses may be neglected [20]. Similarly, as discussed in [21], separating the total losses into components proposed above is of little significance to both the electrical design engineer and the customer.

Therefore, the authors resorted to a more holistic approach, which is primarily based on measurements and post processing of experimental data using FEM software. Apart from the reasons mentioned above, the main motivation for this approach is a very accessible measurement procedure, which is embedded in the transformer production process. Furthermore, the entire post-processing aspect is very simple and not computationally intensive.

IV. MEASUREMENT OF LOSSES AND FLUX DENSITY DISTRIBUTION

This section will discuss all aspects of loss measurement and measurement of all flux density vector components in various core configurations.

A. TEST SET-UP

To simplify the measurement circuit as much as possible, the open core has to be tested separately, which also entails the application of low voltage. As significant ampere turns are necessary to magnetize the open core (usually done from high voltage side), the current needed to drive the excitation from the low voltage side is in the range of several tens to several hundreds of amperes. Thus, measures need to be implemented when constructing the excitation winding, as it has to exhibit negligible temperature rise during testing (typical duration of 15 to 30 minutes).

The excitation winding consists of two parallel, insulated multistrand litz copper conductors, carefully constructed to nullify any circulating current, while still allowing a series-parallel reconnection. The winding is placed on the open core, and connected into an electrical circuit shown in Fig. 2(a). The circuit source is a regulating supply transformer, capable of supplying 120 A of current at a voltage of 750 V. Current, voltage, loss, power factor and frequency measurements are obtained through a calibrated wattmeter model GWINSTEK GPM-8212 cl. 170056, with declared tolerances of $\pm 0.1\%$, $\pm 0.1\%$ and $\pm 0.2\%$ for current, voltage and power readings, respectively. The test setup is shown in Fig. 2(b). To measure the magnitude of flux density vector components, search coils were placed around each test object. In order to measure all three components of the flux density vector, two types of search coils were necessary. Search coils of either type are shown in Fig. 2(c). Type I search coils used to measure the flux density vector component B_L, while Type II coils were

TABLE 1. Search coil designations and location relative to the bottom of the model.

Models 1 and 2				Models 3 and 4			
Type I search coil designation	Type I search coil position [mm]	Type II search coil designation	Type II search coil position [mm]	Type I search coil designation	Type I search coil position [mm]	Type II search coil designation	Type II search coil position [mm]
A1	90	W, X, Y, Z 1	55	A1	25	W, X, Y, Z 1	125
A2	250	W, X, Y, Z 2	215	A2	160	W, X, Y, Z 2	285
A3	410	W, X, Y, Z 3	375	A3	320	W, X, Y, Z 3	445
A4	570	W, X, Y, Z 4	535	A4	480	W, X, Y, Z 4	605
A5	730	W, X, Y, Z 5	695	A5	640	W, X, Y, Z 5	765
A6	825	-	-	A6	800	-	-

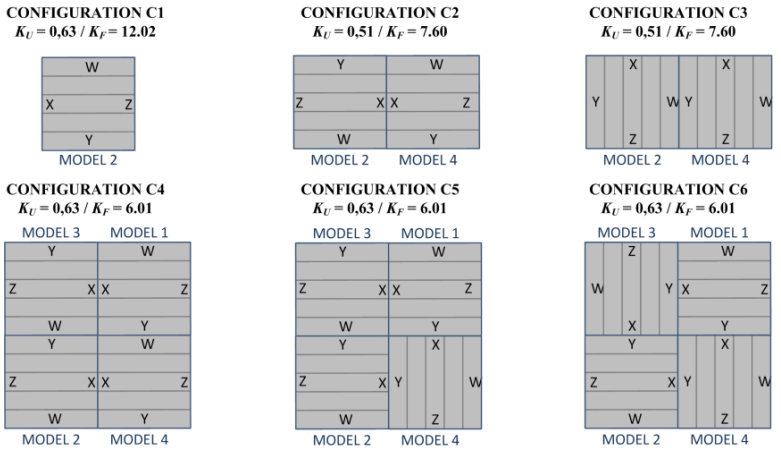

FIGURE 3. Core configurations considered.

used to measure B_T and B_N components, respectively. Each type of coil had 2 turns of insulted litz wire with a total diameter of 0.5 mm. Search coils with a similar turn number were also used in [20] and [22].

The average diameter of Type II coils was 30 mm, while the opening of the Type I search coils was 50 x 50mm. The total added air gap due to coil thickness was ≈1.5 mm. The leads from all search coils were brought to a common measurement terminal board, which allowed simultaneous measurement of six search coil readings using six identical, calibrated digital Multimeters AGILENT 34401A.

Measurement points were controlled through measured voltage and magnetizing current value, obtained beforehand using calculations described in [5]. The frequency value was controlled, and no significant effect was noted in the range of ±0.5 Hz with respect to the rated frequency. Also, the deviation of the magnetic flux density derivative from sine wave was negligible, which was observed in [23] as well. The test object and the excitation winding were elevated for approximately 600 mm, and the containment area of 2 m in diameter was cleared of any residual objects, parts and equipment, as recommended in [24].

B. CORE CONFIGURATIONS CONSIDERED

The test objects were scaled-down models of open cores, representative of actual cores installed in commercial units. Each model consisted of a total of 138 laminated M140-35S sheets. To simplify measurements and calculation processes, the core models were symmetric.

The position of the excitation winding with respect to the core is also comparable to that in an actual PVT. Individual core model fully equipped with search coils can be seen Fig. 2(c). A total of 4 models were assembled and tested. Each model was equipped with 6 Type I search coils and 5 Type II search coils on each side (sides were denoted with W, X, Y and Z respectively), resulting in a total of 26 search coils per model. Search coils placed on W and Y sides served to obtain the flux density vector normal component B_N. Coils on sides X and Z served to obtain flux density vector tangential component B_T. Coils A1 – A6 were used to determine the flux density vector component B_L. Coil locations, given relative to the bottom of the core model, are disclosed in Table 1. Coil positions differ between the models in order to eliminate overlap when the models are assembled together to form different core configurations.

A total of 6 different configurations, labeled C1 – C6, were investigated within the scope of this paper. Each of the configurations simulates different flux orientation patterns and/or core geometry. Fig. 3 shows a cross-section view of each configuration along with orientation of each model. The equivalent FEM model is shown in Fig 4, and will be explained in more detail in section V.

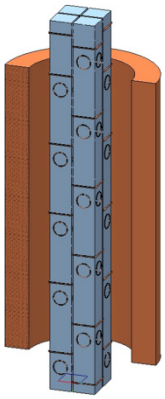

FIGURE 4. Model for configurations C4–C6.

Two different sets of data were measured for each configuration.

The first is the U-I_0-P dataset, with U being the applied voltage, I_0 the current necessary to magnetize the circuit and P total measured losses of the entire setup. This data set is later needed to obtain specific loss curves for each core configuration.

The second dataset is measured induced voltage in each search coil, used to obtain the magnitude of different flux density vector components. These values are later compared with calculated values to prove and verify the overall flux density distribution, which is necessary to determine the referent value of average flux density B_a within the core for each measurement or calculation point.

C. PRELIMINARY MEASUREMENTS

Fig. 5 discloses obtained measurements for both datasets. Due to a very large number of measurements, only those which are necessary to demonstrate key information were included in the paper.

Fig. 5(a) shows the initial measured values of the magnetizing current for each core configuration considered. The measurements are contrasted with results obtained by FEM solver beforehand. The average difference was roughly 2% for all testing points. Results of configurations C3, C5 and C6 are left out, as they are identical to measurements obtained on configurations C2 and C4, as the magnetizing current depends almost solely on the core air path [5].

Fig. 5(b) shows total measured losses for each core configuration. These values are used to obtain specific loss curves for every setup. Prior to these measurements, each model was tested individually. Recorded average deviation between measurements on individual models was below 1%, thus they are considered identical.

Fig. 5(c) shows voltages obtained through readings on search coils for core configuration C1. The main comparison of results will ensue in the next section, so other configurations are not shown here. From readings on search coils A1 – A6, it can be observed that the measured voltage, and consequently the flux density distribution is not uniform

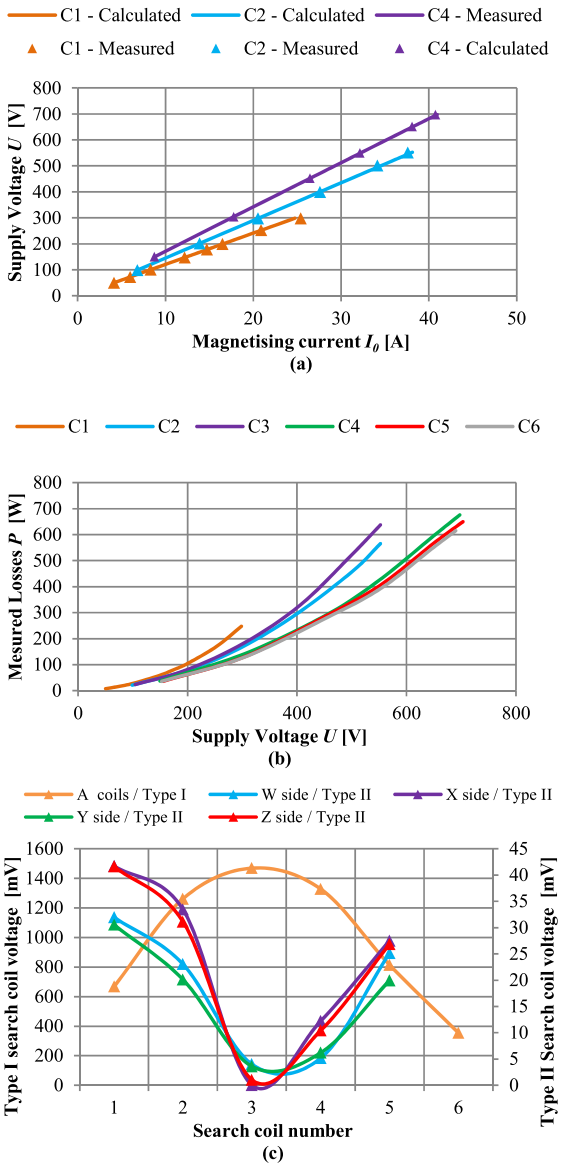

FIGURE 5. (a) Comparison of measured and calculated magnetizing current I_0 for different core configurations (b) Measured loss curves for different core configurations (c) Search coil measurements for configuration C_1 at a supply voltage of 200 V.

along the core height, which is a consequence of the fringing effect occurring at either core end.

It is obvious that the magnitudes of both normal B_N and tangential components B_T are highest at either core end, where the resultant flux density vector strays the most from the lamination orientation direction, as shown in Fig. 1(b). B_L has the lowest magnitude at the core end, which is also logical. On the other hand, both B_N and B_T are practically zero in the middle of the core height where the flux is parallel with the lamination orientation direction, resulting in highest magnitude of B_L component.

Flux distribution is practically identical on the opposite core sides, and any difference in coils marked Y and W and X and Z can be attributed to measurement inaccuracy or

imperfect coil alignment. It can also be concluded that all four core sides exhibit similar flux distribution. However, weak anisotropic behavior is noticeable between X-Z and Y-W coil sides, similar to what was observed in [16]. All measurements conducted showcased the same trend.

V. DETERMINATION OF AVERAGE FLUX DENSITY

Numerical modeling using Infolytica MagNet was performed to correlate measured losses to average flux density at each measurement point. Every calculation was performed as a full-scale 3D static non-linear model [25].

To calibrate the numerical model different values of relative permeability μ_r were used, ranging from 15000-35000. These are derived characteristics obtained from core manufactures and the authors' previous experience.

The anisotropic effect was modeled using equivalent permeability tensor shown in equation (4). Permeabilities μ_L, μ_N and μ_T were defined according to equations (5) - (7).

$$[\mu] = \begin{bmatrix} \mu_L & 0 & 0 \\ 0 & \mu_T & 0 \\ 0 & 0 & \mu_N \end{bmatrix} \tag{4}$$

$$\mu_L = (1-F)\,\mu_0 + F\,\mu_{fL} \approx F\,\mu_{fL} \tag{5}$$

$$\mu_N = \mu_{fN}/(F + (1-F)\,\mu_{fN}/\mu_0) \tag{6}$$

$$\mu_T = (1-F)\,\mu_0 + F\,\mu_{fT} \approx F\,\mu_{fT} \tag{7}$$

In the above equations F is the stacking factor and μ_{fL}, μ_{fN} and μ_{fT} are core sheet permebilities in lamination, normal and tangential directions, respectively [7].

The best results were obtained when the permeability in the μ_{fN} was defined as roughly one thousandth part of the permeabilities in the other two directions. Of course, due to shifting magnetic orientations in configurations C2 – C6, μ_N and μ_T refer to local coordinate systems of each core model.

Excitation winding and search coils were modeled as stranded copper objects. Example of the numerical model for configurations C4 - C6 can be seen in Fig. 4.

All calculations were performed on an Intel Core i7-2630QM CPU with 2.0 GHz per core and 16 GB of RAM, typically lasting between 25 and 40 minutes, depending on the number of core models and search coils.

All configurations were analyzed at two predetermined average flux density B_a values, 0.5 T and 1T. The results for both measurement points are linearly proportional, so only the latter will be presented.

The comparison of measured and calculated results for the most complex configuration C6 at an estimated average flux density B_a of 1T is shown in Fig. 6.

Comparison of Type I coil readings for models 1 and 3 is shown in Fig. 6(a). The average difference in Type I coil readings between identical models (i.e. 1 and 2, 3 and 4) is roughly 2%. As it can be seen, the calculated and measured values correspond very well. The average deviation between the result sets is roughly 3%, which is a very good result.

Fig. 6(b) and 6(c) show the readings from Type II coils for models 1 and 3, respectively. The deviation in measurements

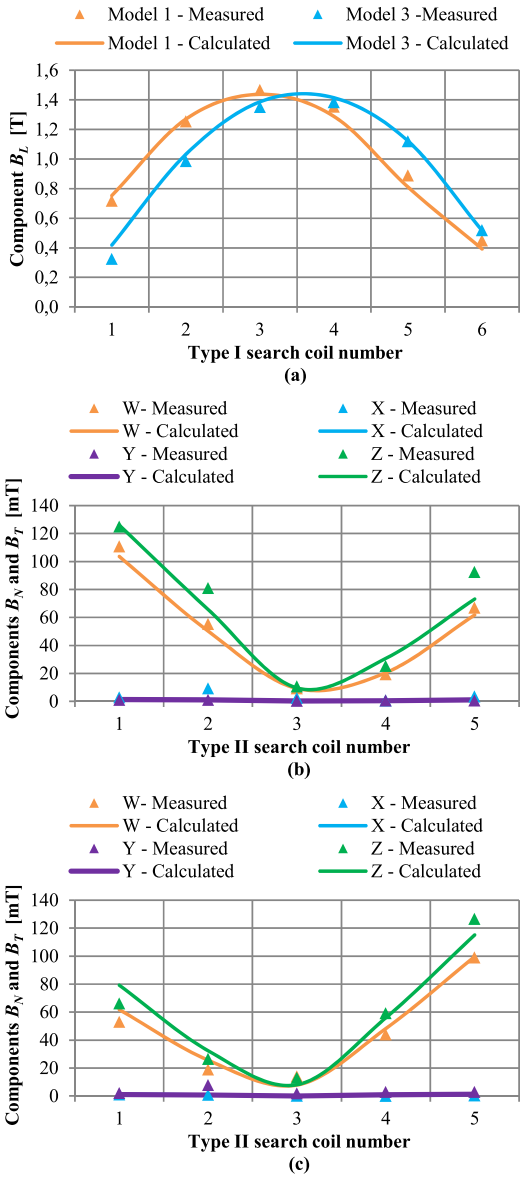

FIGURE 6. Comparison of flux density vector component calculation and measurement for configuration C6 (a) Component BL for Model 1 and 3 (b) Components B_N and B_T for Model 1 (c) Components B_N and B_T for Model 3.

between identical models is between 10 and 12%, respectively, which is larger than with Type I coils,. The higher degree of inaccuracy for Type II coils is expected as the magnitude of B_N and B_T flux components are considerably smaller than the magnitude of B_L component.

Similar error margin increase is noticeable when comparing the readings from Type II coils with calculated results. The average deviation for sides W and Z, which represent the lamination-air boundary, was 7 and 14%, respectively. It can be observed that the magnitude of B_N and B_T on core interconnections (sides Y and X) is practically zero. This shows that the insertion of a lateral air gap due to search coil placement did not significantly disrupt the flux distribution.

TABLE 2. Search coil flux density deviation between measurements and calculation.

Search coil position	Δ [%]					
	C1	C2	C3	C4	C5	C6
A	2.56	2.78	2.69	3.12	3.44	3.00
W	4.68	5.46	6.35	12.19	6.89	5.92
X	5.96	-	7.06	-	-	-
Y	4.87	8.12	6.44	9.19	9.86	-
Z	6.06	7.65	5.86	5.99	13.15	10.12

The weak anisotropy mentioned in previous sections is also noticeable in Fig. 6, with the average difference in readings between W and Z sides being roughly 27%, which is in line with the results shown in Fig. 5(c). Identical behavior was recorded between Models 2 and 4.

The results of all other configurations tested are presented in Table 2, expressed as average deviation of measured and calculated flux density per model in each configuration. Expression used in this evaluation is shown in equation (8).

$$\Delta = \left| \frac{B_m}{B_c} - 1 \right| \cdot 100[\%] \tag{8}$$

In equation (8), B_m is the measured flux density, while B_c is the calculated, regardless of the flux density vector component. Both were obtained through integration over the cross sectional area of each search coil [16], [22]. The results from the search coils with the same designation were then averaged. Search coils on core interconnections were excluded from Table 2, as their readings are essentially zero.

The margin of error shown in Table 2 is acceptable and verifies the numerical calculation.

Furthermore, it can be concluded that the contribution of the B_L component to the average flux density is considerably larger than that of B_N and B_T components.

The next step is to determine the average flux density B_a distribution along the core. To be able to compare calculation to measurement, the calculation of B_a was done in plane of each Type I coil. B_a was obtained through integration over the core segment in the observed plane. The comparison of these results for models 1 and 3 in configuration C6 is given in Fig. 7(a) and 7(b), respectively.

The average difference between calculation and measurements is between 3 and 8 %. The same range of errors was observed with configurations C1 – C5.

These results were also compared with results obtained through numerical calculation with isotropic material properties, as this saves computational time and requires a less refined mesh. The comparison of results obtained by calculation with isotropic material is also shown in Fig. 7.

It can be concluded that these two result sets are interchangeable, with the same error margin.

This also simplifies the calculation of average flux density within the core, as instead of numerical integration over every core model, average core flux density can be determined from flux density contour plot, along the mean flux path length l_{Fe}, defined by equation (3). It was also found that the position

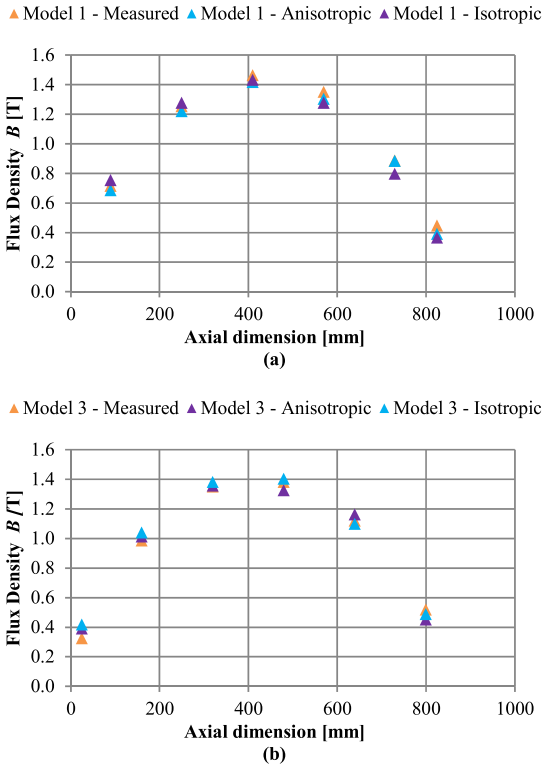

FIGURE 7. Comparison of average flux density B_a in plane of Type I search coils (a) C6 - Model 1 (b) C6 – Model 3.

of the line can be arbitrary, as long as sufficient number of plot points is defined (typically 500 or more, depending on model size).

It was disclosed earlier that all measurements that included the search coil voltage dataset were performed at two distinct flux densities, 0.5 and 1T. The average densities, denoted as B_a, for all configurations calculated according to procedure disclosed above were in the range of [0.51-0.54] T and [1.02-1.05] T, respectively, which shows that the measurement points were adequately selected.

VI. AVERAGE LOSS CURVE CONSTRUCTION

So far, total losses and average flux densities were determined. To bring the two into correlation, first it is necessary to extract the core losses P_c from the total measured losses P_m. This is done through equation (9)

$$P_c = P_m - I_0^2 R \quad P_{spec} = \frac{P_c}{m_c} \tag{9}$$

I_0 is the measured value of the magnetizing current and R is the resistance of the excitation winding, m_c is the core mass, routinely measured by the core manufacturer.

Once B_a is known at every measured point, final specific loss $P_{spec} = f(B_a)$ curves can be constructed. Every constructed curve may be accurately fitted from processed results with a 2nd order polynomial as shown in equation (10).

$$P_{spec}(B_a) = X \cdot B_a^2 + Y \cdot B_a \tag{10}$$

As a part of the transformer production process, every core is subjected to the above mentioned methodology, resulting in multiple data sets for each design. The final curves for each data set are then averaged in order to obtain a referent curve for each core design. This way, two things are achieved; a more accurate referent curve for each core and in-process quality control, with any deviation from the referent curve clearly visible.

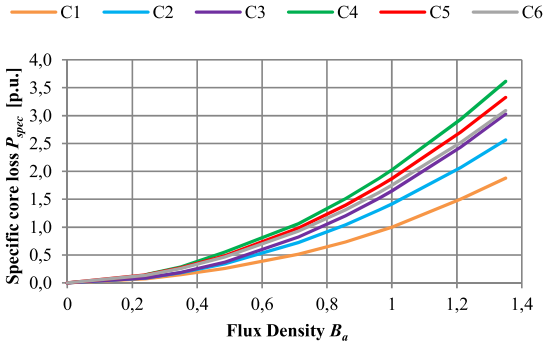

FIGURE 8. Final specific loss curves for all core configurations.

The final specific loss curves, constructed according to the displayed methodology, are shown in Fig. 8 for each core configuration.

There are several important conclusions that can be deduced from Fig. 8, expressed in per unit values in respect to specific losses of configuration C1 at 1T.

Firstly, it is obvious that core configuration has a drastic influence on specific losses P_{spec}. This is the primary reason why the research performed is very significant, as it proves that material curves provided by core steel manufacturers are insufficient and specific losses of every core configuration have to be determined individually.

Secondly, there are several key parameters that determine the specific losses in the open core, including steel material, lamination number, orientation and dimensions, K_U and K_F factors and disposition of the magnetizing winding to the core.

For instance, when comparing loss curves for configurations C2 and C3, it is obvious that C2 exhibits losses lower by 15% on average. When the geometry of the two configurations is compared, it is clear that the normal flux density vector component B_N affects a larger number of core sheets, causing eddy current losses in each of them.

Similarly, when configurations C4, C5 and C6 are compared, it is obvious that by rotating one or two core segments, the path of the normal component of flux density vector was "interrupted" with laminations mostly parallel to its direction, which caused lower total losses. The difference between configurations C5 and C4 is 8.5% and between C6 and C4 13.3% on average.

VII. VERIFICATION

It is clear that this approach cannot be verified directly. Therefore, the presented methodology was applied to cores which were installed in actual PVT units. That way, two sets of measurements obtained in different conditions can be compared.

Referent core losses were obtained from measured no-load losses on completely assembled units and then compared to losses obtained through loss curves constructed using the methodology described above. The testing equipment for the completed units was the same as for the tests performed on core models, and was described in section IV.

A comparison was performed on a total of five PVT units, with rated output spanning from 50 to 150 kVA. Each unit had different core geometry, with K_F and K_U parameters given in Table 3.

TABLE 3. Core parameters of the verification units.

Unit	Designation	K_F	K_U	m_c [kg]
1	145 kV 50 kVA	11.2	0.92	186
2	245 kV 50 kVA	14.8	0.92	227
3	300 kV 150 kVA	17.9	0.92	460
4	362 kV 100 kVA	15.3	0.92	481
5	550 kV 150 kVA	21.5	0.92	571

The magnetization on completed units was done from the primary side, thus rendering the magnetizing current very small, however, the I^2R losses caused by the magnetizing current I_0 were deducted from the measured total so that only core losses are analyzed [5].

The tests were done up to 150% of rated voltage for units 1 through 3, and up to 100% of rated voltage for units 4 and 5. As units 4 and 5 are 362 kV and 550 kV units, respectively, they exceed the rated insulation level of components in the testing circuit at 150% of rated voltage, and were therefore not considered at said voltages.

The comparison of measured and calculated results is shown in Fig. 9. All results were expressed in the same way and are comparable to those in Fig. 8.

The correlation between estimated core losses and losses extracted from no-load measurements is very good in all points tested, with an average deviation of 7%.

The deviation itself may be attributed to different testing equipment, which, when testing the actual unit, has to withstand high voltage stress. Furthermore, the magnetization of the core from the high voltage side is slightly different in comparison to low voltage magnetization using the excitation winding. Lastly, a possible inaccuracy of the measured value of magnetizing current I_0 can also be a contributor, as it is affected by the presence of the main insulation system.

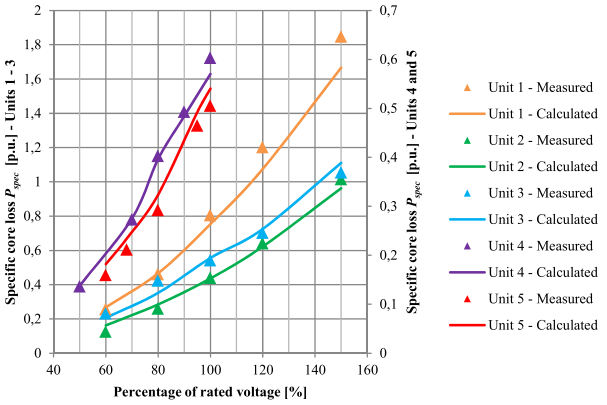

FIGURE 9. Comparison of measured and calculated core losses on actual units.

Nevertheless, the exhibited acceptable error margin is acceptable, and in line with the standard-proposed tolerances on both individual component and total no-load loss values, which serves to prove that the proposed approach can be utilized and applied in actual transformer production [26].

Furthermore, if the results are analyzed in more detail, it is obvious that the value of P_{spec} decreases with the increase of the core form factor K_F. The same trend was observed on tested core configurations C1 – C6, and shown in Fig. 8.

The reasoning behind this occurrence is that cores with a higher form factor have a lower flux fringing effect at either core end, which consequently decreases the values of flux density vector components B_N and B_T, which are the dominant contributor to open core losses, as discussed in section II.

VIII. CONCLUSION

There are three main conclusions that are a result of the research performed.

The displayed methodology showed very good correlation between calculated and measured values of all three flux density vector components B_L, B_N and B_T, respectively. The proposed determination of specific core loss $P_{spec} = f(B_a)$ curves and total core losses was verified on several transformer units, with acceptable error margin. The paper also provides context for open-core losses, their origin and significance.

The proposed test setup can be utilized on various core geometries in order to analyze different open core design parameters, which establishes the proposed approach as an indispensable tool for open-core transformer design. Furthermore, the entire procedure can be seamlessly implemented in design, production and quality control processes of actual transformer units.

Finally, the presented test setup and considered core configurations can be used as a relevant and simple benchmark for different core loss models and calculation methods, as multiple complex occurrences can be analyzed, such as material anisotropy, saturation, and material orientation. The possibilities of the presented setup add value to the concept presented here and serve as a beacon for future work.

REFERENCES

[1] I. Žiger, B. Bojanić, and D. Krajtner, "Power voltage transformers—Expanding beyond station service," in *Proc. IEEE Power Energy Soc. Gen. Meeting*, Denver, CO, USA, Jul. 2015, pp. 1–5.
[2] D. Xu, N. S. Powers, and W. Sae-Kok, "Development of a power source for rural electriciation," in *Proc. IEEE Global Humanitarian Conf. (GHTC)*, Seattle, WA, USA, Oct. 2015, pp. 340–347.
[3] *IEEE Standard Requirements for Instrument Transformers*, IEEE Standard C57.13-2016, Jun. 2016.
[4] I. Žiger, B. Bojanić, and D. Krajtner, "Open-core power voltage transformer: Concept, properties, application," in *Proc. IEEE Int. Energy Conf. (ENERGYCON)*, Cavtat, Croatia, May 2014, pp. 246–253.
[5] I. Žiger, D. Krajtner, Z. Ubrekić, and M. Brkić, "Design of the open-core power voltage transformer," in *Proc. Int. Colloq. Transformer Res. Asset Manage.*, Dubrovnik, Croatia, 2012, pp. 1–12.
[6] A. P. S. Baghel and S. V. Kulkarni, "Modeling of magnetic characteristics including hysteresis effects for transformers," in *Proc. Int. Colloq. Transformer Res. Asset Manage.*, Split, Croatia, 2014, pp. 1–11.
[7] J. Wang, H. Lin, Y. Huang, and L. Huang, "Numerical analysis of 3D eddy current fields in laminated media under various frequencies," *IEEE Trans. Magn.*, vol. 48, no. 2, pp. 267–270, Feb. 2012.
[8] O. Biro, K. Preis, and K. R. Richter, "Various FEM formulations for the calculation of transient 3D eddy currents in nonlinear media," *IEEE Trans. Magn.*, vol. 31, no. 3, pp. 1307–1312, May 1995.
[9] P. Hahne, R. Dietz, B. Rieth, and T. Weiland, "Determination of anisotropic equivalent conductivity of laminated cores for numerical computation," *IEEE Trans. Magn.*, vol. 32, no. 3, pp. 1184–1187, May 1996.
[10] I. Sebestyen, S. Gyimothy, J. Pavo, and O. Biro, "Calculation of losses in laminated ferromagnetic materials," *IEEE Trans. Magn.*, vol. 40, no. 2, pp. 924–927, Mar. 2004.
[11] K. Preis, O. Biro, and I. Ticar, "FEM analysis of eddy current losses in nonlinear laminated iron cores," *IEEE Trans. Magn.*, vol. 41, no. 5, pp. 1412–1415, May 2005.
[12] H. Kaimori, A. Kameari, and K. Fujiwara, "FEM computation of magnetic field and iron loss in laminated iron core using homogenization method," *IEEE Trans. Magn.*, vol. 43, no. 4, pp. 1405–1408, Apr. 2007.
[13] X. Yan, X. Yu, M. Shen, D. Xie, and B. Bai, "Research on calculating eddy-current losses in power transformer tank walls using finite-element method combined with analytical method," *IEEE Trans. Magn.*, vol. 52, no. 3, Mar. 2016, Art. no. 6300704.
[14] M. T. Kakhki, J. Cros, and P. Viarouge, "New approach for accurate prediction of eddy current losses in laminated material in the presence of skin effect with 2-D FEA," *IEEE Trans. Magn.*, vol. 52, no. 3, Mar. 2016, Art. no. 6300604.
[15] L. Wang, W. Chen, D. Tao, W. Li, and B. Ge, "Research on the impact of screen properties on eddy current and flux in end region of a large air-cooled turbo-generator," *IEEE Trans. Energy Convers.*, vol. 31, no. 1, pp. 218–227, Mar. 2016.
[16] Z. Cheng *et al.*, "Effect of excitation patterns on both iron loss and flux in solid and laminated steel configurations," *IEEE Trans. Magn.*, vol. 48, no. 8, pp. 3185–3188, Aug. 2010.
[17] Z. Cheng *et al.*, "Effect of variation of B-H properties on loss and flux inside silicon steel lamination," *IEEE Trans. Magn.*, vol. 47, no. 5, pp. 1346–1349, May 2011.
[18] E. Hajipour, P. Rezaei, M. Vakilian, and M. Ghafouri, "Power transformer no-load loss prediction with FEM modeling and building factor optimization," *J. Electromagn. Anal. Appl.*, vol. 3, no. 10, pp. 430–438, 2011.
[19] I. Hernandez, J. C. Olivares-Galvan, P. S. Georgilakis, and J. M. Cañedo, "Core loss and excitation current model for wound core distribution transformers," *Int. Trans. Electr. Energy Syst.*, vol. 24, no. 1, pp. 30–42, 2014.
[20] F. Marketos, D. Marnay, and T. Ngnegueu, "Experimental and numerical investigation of flux density distribution in the individual packets of a 100 kVA transformer core," *IEEE Trans. Magn.*, vol. 48, no. 4, pp. 1677–1680, Apr. 2012.
[21] J. Lorenz, "Electrical machine iron loss predictions—A unique engineering approach utilizing transient finite-element methods—Part II: Application and validation," *IEEE Trans. Ind. Appl.*, vol. 50, no. 4, pp. 2871–2875, Jul./Aug. 2014.

[22] I. Šulc and Z. Valković, "Flux distribution inside the transformer core in short circuit," in *Proc. Int. Colloq. Transformer Res. Asset Manage.*, Dubrovnik, Croatia, 2012, pp. 1–7.
[23] W. A. Pluta, "Angular properties of specific total loss components under axial magnetization in grain-oriented electrical steel," *IEEE Trans. Magn.*, vol. 52, no. 4, Apr. 2016, Art. no. 6300912.
[24] I. Franjić, "Magnetic characteristic of pole-type voltage transformer cores," M.S. thesis, Dept. Elect. Eng., Zagreb Univ. Appl. Sci., Zagreb, Croatia, 2011.
[25] (May 2017). *MagNet and MotorSolve BLDC: Electromagnetic Field Simulation Software*. [Online]. Available: http://www.infolytica.com
[26] *IEEE Standard for General Requirements for Liquid-Immersed Distribution, Power, and Regulating Transformers*, IEEE Standard C57.12.00-2015, Dec. 2015.

IGOR ŽIGER (M'14) was born in Zagreb, Croatia, in 1986. He received the B.Sc. and Univ. Spec. Transf. degrees from the Faculty of Electrical Engineering and Computing, University of Zagreb, Croatia, in 2009 and 2015, respectively.

Since 2010, he has been an Electrical Design and Research and Development Engineer with Končar–Instrument transformers Inc., where he is currently the Electrical Design Department Manager. His main professional and research interests lie in the field of high-voltage instrument transformer analysis, insulation design, and transformer losses.

BOJAN TRKULJA was born in Bjelovar, Croatia, in 1978. He received the B.Sc., M.Sc., and Ph.D. degrees in electrical engineering and computing from the University of Zagreb, Zagreb, Croatia, in 2001, 2004, and 2008, respectively.

He is currently an Associate Professor with the University of Zagreb. His main research interests include the application of numerical methods in electromagnetic field analysis.

ŽELJKO ŠTIH was born in Krapina, Croatia, in 1955. He received the Ph.D. degree from the Faculty of Electrical Engineering and Computing, University of Zagreb, Zagreb, in 1984.

He is currently a Full Professor with the Faculty of Electrical Engineering and Computing, University of Zagreb, teaching the electromagnetic field theory and numerical methods. His research interests include computational electromagnetism and its application in power apparatus and systems.